Enhancing luminous transmittance and hysteresis width of VO_2-based thermochromic coatings by combining GLAD and RGPP approaches

A.J. Santos[a,b,c,*], N. Martin[c], J.J. Jiménez[a,b], R. García[a,b], F. M. Morales[a,b]

[a] *IMEYMAT: Institute of Research on Electron Microscopy and Materials of the University of Cádiz, E-11510, Puerto Real, Spain.*

[b] *Department of Materials Science and Metallurgic Engineering, and Inorganic Chemistry, Faculty of Sciences, University of Cádiz, E-11510 Puerto Real, Spain.*

[c] *Université de Franche-Comté, CNRS, Institut FEMTO-ST, F-25000 Besançon, France.*

* Corresponding author: antonio.santos@uca.es

Abstract: This work reports on alternative strategies for improving the performance and thickness uniformity of VO_2-based thermochromic coatings by atmospheric oxidation of zig-zag vanadium films sputtered at glancing angles in presence of reactive oxygen. With the aim of scrutinizing the effect of deposition parameters, VO_{2-x} films of 25, 50 and 100 nm nominal thickness were deposited on glass substrates, sometimes without reactive oxygen, sometimes by injecting oxygen pulses for 4 or 8 s every 16 s of deposition. Comprehensive structural, compositional and functional characterizations of samples annealed at reaction temperatures between 475–550°C for times ≤ 60 s confirmed the synthesis of the VO_2(M) phase and the development of singular microstructural and thermochromic features depending on the duration of the oxygen injection pulses. Here, it was evidenced that longer oxygen pulses lead to significantly higher luminous transmittances and broader hysteresis loops thanks to the formation of generally larger grains, although with heterogeneous morphology and size distribution.

These same events also caused unwanted increases in the metal-to-insulator transition temperature and the occurrence of asymmetric hysteresis loops. Optimal performances for smart glazing applications were eventually achieved by instantaneous oxidation of 25 nm thick films deposited with 8 s oxygen pulses, exhibiting remarkable luminous transmittances (>55%), solar modulation abilities (>5%), beneficial drops in critical temperature without doping (up to 7°C below the standard value for pure VO_2) and extraordinarily wide variable hysteresis of between 18–26°C. These results represent a substantial enhancement, mainly regarding visible transmittance and hysteresis width, over those attained through similar two-step approaches, paving the way for further doping processes.

Keywords: Vanadium dioxide, glancing angle deposition, reactive gas pulsing process, rapid thermal annealing, Vis-NIR spectrophotometry, thermochromism, smart glazing

1. Introduction

Energy saving and further integration of renewable energy sources are critical issues to be addressed in a real-world transition towards sustainable smart cities[1]. Most of the actions taken to face this global challenge have focused on buildings, and more particularly on windows, which are responsible for large energy losses as a result of the high heat transfer coefficients of glazing involved in their structure[2]. In this framework, passive smart windows based on vanadium dioxide (VO_2) are emerging as one of the most viable future alternatives to improve energy efficiency of buildings[3–7]. The particularity of this material lies in its thermally induced reversible metal-to-insulator transition (MIT) at temperatures around 68ºC (T_c), which gives rise to a distortion of the crystalline structure from monoclinic (M1), with high transparency in the near-infrared (NIR) at low temperature, to thermal insulator rutile (R) at temperatures above T_c[8–10]. This phenomenon allows VO_2-based coatings to control the solar radiation that enters into a building depending on the outside temperature while minimally affecting its visible transmittance, which is a natural way of conditioning. Nevertheless, the real deployment of this technology is being delayed for two main reasons: (i) the complexity and high cost involved in the large-scale transfer of the current VO_2 manufacturing strategies; and (ii) the difficulty of reaching an appropriate balance between optical and thermochromic performances while satisfying the minimum requirements for smart windows applications.

On the one hand, the large number of oxidation states of vanadium, which in turn is aggravated by the existence of more stable oxidized compounds such as V_2O_3 or V_2O_5 as well as different polymorphs of the same oxide[11–15], makes the reaction window for VO_2 synthesis very narrow. This results in fabrication processes involving the establishment of very rigid conditions with oxidizing/reducing atmospheres or vacuum

at high temperatures during prolonged oxidation times[16–19]. Recently, several authors have started to adopt more scalable strategies based on post-deposition air oxidation of vanadium thin films[20–24]. However, in most cases, either precise control of such fundamental reaction parameters as heating and cooling rates has been overlooked, or substrates unsuitable and/or expensive for smart window applications (e.g. quartz, sapphire, silicon) have been used. In this context, our previous works have shown that, thanks to the precise control of annealing parameters, the fabrication of VO_2-based films on glass substrates can be achieved through a simple two-step approach consisting of the rapid air oxidation of porous vanadium films achieved through the Glancing Angle Deposition (GLAD) technique[25,26]. Nonetheless, although it has been evidenced that the implementation of these nanostructures significantly enhances the reactivity and selectivity of such coatings, it should be noted that the large-scale manufacturing of single-layer GLAD films results in inhomogeneous layer thicknesses[27,28], which represents a major drawback. Likewise, these former studies only focused on V-GLAD films, leaving unexplored the effect that the use of VO_{2-x} (combinations of V and O with O/V ratios between 0 and 2) precursor mixtures may have on the final performance of the VO_2-based films accomplished by following the same two-step procedure.

On the other hand, the practical application of these coatings is conditioned by simultaneous requirements of solar modulation ability (ΔT_{sol}) and luminous transmittance (T_{lum}) above 10% and 60%, respectively[3–5,29], which fulfillment is far from being straightforward given the antagonistic relationship between these two parameters (i.e. thicker VO_2 films result in better ΔT_{sol} values, but at the expense of decreasing T_{lum}). Another key limitation is the relatively high temperature at which the reversible MIT is thermally induced. In order to reduce this parameter to 25–30°C,

doping of vanadium dioxide films with transition metal cations has been researched, with tungsten being the most common additive[3,30–32]. However, the incorporation of dopants, even in very small quantities, also leads to progressive and joint decreases of ΔT_{sol} and T_{lum}. In this regard, it is worth highlighting the role of the hysteresis width (W_H), a parameter that is normally neglected in the design and manufacture of smart windows and which could somehow compensate the performance of coatings with moderate critical temperatures while mitigating the adverse effects of using larger quantities of dopant. Considering the amount of solar radiation absorbed by a window glass during a sunny summer day in regions relatively close to the equator[33], it is reasonable to think that the thermal blocking of a thermochromic VO_2-based coating could be activated at temperatures between 40–45ºC, so that a wider hysteresis (i.e. W_H > 15ºC) would allow this blocking to be maintained up to temperatures at which the heat is not unbearable (20–25ºC). Unlike what would be expected for a narrow hysteresis, this would therefore allow the temperature inside a building to be conditioned.

In order to further optimize the two-step approach developed in our previous research for the fabrication of VO_2-based thin films, the present work aims not only to tackle some of the inherent weaknesses of the proposed methodology, but also to carry out a comprehensive study on the effect of the different deposition parameters on the final performance and properties of the coatings after oxidation in air atmosphere. For this purpose, direct current (DC) magnetron-sputtered VO_{2-x} films with zig-zag arrangement and of 25, 50 and 100 nm nominal homogeneous thickness were deposited on glass substrates by combining GLAD and a Reactive Gas Pulsing Process (RGPP). Subsequently, VO_2-based thermochromic coatings were achieved through highly controlled atmospheric rapid annealing of VO_{2-x} samples at different temperatures (T_r)

and reaction times (t_r) depending on the volume of material to be oxidized. Micro/nano-structural and compositional analyses of as-deposited and oxidized samples were performed by combining scanning electron microscopy (SEM), grazing incidence X-ray diffraction (GIXRD), and scanning-transmission electron microscopy (S)TEM techniques, including high-angle annular dark-field (HAADF) and high-resolution (HRTEM) imaging, as well as energy-dispersive X-ray (EDX) and electron energy-loss (EELS) spectroscopies. The process-structure-property relationships for the synthesized surfaces were eventually determined by variable temperature Vis-NIR spectrophotometry and resistivity measurements, paying special attention on the effects that zig-zag nanostructuring and oxygen injection times have not only on the resulting thermocromic features along the metal-to-insulator transition, but also on the parameters of interest for smart window applications (T_{lum}, ΔT_{sol}, T_c, W_H).

2. Materials and Methods

2.1. Deposition process

The films were deposited at room temperature by DC magnetron sputtering from a vanadium metallic target (51 mm diameter and 99.9 atomic % purity) in a homemade deposition chamber. It was evacuated down to 10^{-5} Pa before each run by means of a turbomolecular pump backed by a primary pump. The target was sputtered with a constant current density of J = 100 A m^{-2}. Glass substrates (Menzel Gläser ® microscope slides) were placed at a distance of 65 mm from the target center. On the basis of our previous studies[34], porous VO_{2-x} films with large surface-to-volume ratios and enhanced reactivity with oxygen were deposited by combining GLAD and RGPP techniques. The deposition angle α (average angle of incoming particle flux) relative to the substrate normal was set at α = 85º (the maximum inclination allowed for

efficient GLAD deposition, so that the greater the deposition angle, the higher the overall porosity of the film and, therefore, its specific surface area[35]) with no rotation of the substrate (i.e., $\phi = 0$ rev h^{-1}). Argon was injected at a mass flow rate of 2.40 sccm and the pumping speed was maintained at S = 13.5 L s^{-1}, whereas the oxygen gas was periodically supplied into the sputtering chamber. A rectangular pulsed signal was employed for the oxygen flow rate with respect to time evolution. The pulsing period was set at P = 16 s. The maximum oxygen flow rate was q_{O2Max} = 0.40 sccm. It corresponds to the critical flow required to avalanche the process in the compound sputtering mode. The minimum oxygen flow rate was q_{O2min} = 0 sccm. Thus, oxygen injection times (t_{ON}) of 0, 4 and 8 s were used. These operating conditions gave rise to a total sputtering pressure changing slightly between 3.00–3.08 × 10^{-3} mbar and a target potential from 307 to 324 V, which do not disturb the growth mechanisms of the GLAD process. Different VO_{2-x} nominal thicknesses (25, 50 and 100 nm) were achieved by adjusting the deposition time according to average deposition rates of 240, 285, and 210 nm h^{-1} for t_{ON} = 0, 4 and 8, respectively, which were previously determined for α = 85º[34]. At half the time required to achieve any given layer thickness, the samples were subjected to an azimuthal rotation of $\Phi = 180°$ to promote the fabrication of zig-zag GLAD films of uniform overall layer thickness.

2.2. Thermal treatments

After deposition, vanadium samples were thermally treated in a homemade reaction system. It consists in an Al_2O_3 tube on a furnace with SiC resistors able to reach temperatures of up to 1500°C, with an attached concentric steel tube and a high temperature steel-covered K-type thermocouple inside. This thermometer bar acts as an axle for a system of horizontal translation. At the end of the metallic tube nearby the furnace, the thermocouple crosses and fixes to a cylinder placed inside this tube,

mechanized with a hitch to hang a combustion boat. Thus, the thermometer tip is always placed some millimeters over the center of this boat, which is an alumina crucible, allowing the temperature in the reaction zone to be monitored. The other end side also crosses and is fixed to another piece that is part of a handlebar used to slide the specimen holders inside and outside the furnace. In this way, by fixing a temperature in the center of the furnace, one is able to control the temperature increase (heating rate) by moving the boat more and more inside the furnace (for a more detailed overview of the reaction system, refer to previous studies[36,37]). Consequently, translation routines were prepared for reaching an average heating rate of 42ºC s^{-1}, as well as for adjusting longer or shorter reaction times at a desired temperature. Lastly, all samples were left to be cooled down in air to room temperature.

2.3. Structural, compositional and functional characterizations

Topographic micrographs of as-deposited and oxidized samples were acquired using a Thermo Scientific Scios 2 DualBeam analytical focused ion beam scanning electron microscopy (FIB-SEM) system operating at 5 kV. This same facility was also used to prepare electron-transparent cross-section lamellae for (S)TEM observations. High-resolution transmission electron microscopy (HRTEM) and high-angle annular dark-field imaging (HAADF) studies were carried out in a Thermo Scientific TALOS F200X G2 analytical microscope working at an accelerating voltage of 200 kV. The energy-dispersive X-ray spectroscopy (EDX) studies were carried out in this same microscope using a Super-X detection system that is constituted by four silicon drift detectors distributed around the sample to be analyzed. On the other hand, the spatially-resolved electron energy-loss spectroscopy (EELS) experiments were carried out in a FEI Titan^3 Themis 60-300 aberration-corrected microscope, which allowed to incorporate a monochromator (Gatan Quantum ERS 966) in the electron gun to improve the energy

resolution down to about 0.25 eV while using a 0.05 eV/channel energy dispersion. With a 5 mm diameter aperture inserted, the convergence and collection semi-angles were set to 21.5 and 75.3 mrad at a camera length of 29.5 mm, respectively, while using a probe current of between 30 and 140 pA depending on the experiment. Dwell times of about 0.25 seconds per pixel were set during the spectrum imaging experiments, which were carried out under Dual EELS mode to record nearly simultaneously both the low-loss signal and the V-$L_{2,3}$ and O-K high-loss edges, at each pixel position. GIXRD scans were performed on a Malvern Panalytical Aeris diffractometer (Cu radiation) working at 30 kV (10 mA) and setting a grazing incidence angle of 0.8°. The thermochromic optical behavior of the prepared VO_2–based films was determined via transmission spectroscopy using a PerkinElmer Lambda 900 UV/VIS/NIR Spectrometer equipped with a THMS600 Linkam stage for temperature control. Vis-NIR transmittance spectra were recorded in the wavelength range of 350–2500 nm at selected temperatures in the range of 25–90ºC. For the dynamic monitoring of the thermally induced phase transition, the thermal evolution of the optical transmittance at a selected NIR wavelength (2000 nm) was observed in both heating and cooling cycles at a controlled rate of 5 °C min^{-1}. DC electrical resistivity versus temperature measurements of the oxidized films were performed in a custom-made chamber. It is covered in order to have a dark environment, using the four-probe van der Pauw geometry in the temperature range of 25–90ºC with a ramp of 2°C min^{-1} and then back to 25°C with the same negative ramp. Humidity and cleanness were considered as constant. The error associated to all the resistivity measurements was always below 1% and the quality of the contacts was checked prior to every run (i.e. I/V correlation close to 1) to ensure that ohmic contacts were attained (use of gold coated tips).

3. Results and discussion

3.1. Morphology, structure and composition of as-deposited and annealed films

VO_{2-x} zig-zag GLAD samples of 25, 50, and 100 nm nominal thickness were sputtered using oxygen injection times of 0, 4, and 8 s. Thereupon, all of them were subjected to the atmospheric thermal treatments previously determined as optimal for each of the layer thicknesses considered[25,26], which involve reaction temperatures between 475–550ºC and times below 60 s. All the samples addressed in the present study, classified according to their deposition and annealing conditions, are collected in **Table 1**.

Table 1. Deposition and thermal treatment conditions for the samples addressed in this study. τ_N is the nominal layer thickness, T_r is the reaction temperature, t_r is the reaction time, and t_{ON} is the oxygen injection time.

Sample	τ_N (nm)	T_r (ºC)	t_r (s)	t_{ON} (s)
S100_475_1	100	475	60	0
S100_475_2				4
S100_475_3				8
S100_550_1		550	5	0
S100_550_2				4
S100_550_3				8
S50_475_1	50	475	30	0
S50_475_2				4
S50_475_3				8
S50_550_1		550	1	0
S50_550_2				4
S50_550_3				8
S25_500_1	25	500	1	0
S25_500_2				4
S25_500_3				8

In order to investigate the effect of the different manufacturing parameters on the resulting microstructures more clearly, only samples with a nominal thickness of 100

nm will be addressed in this section. Together with having a larger volume of material and more apparent zig-zag architectures, this will subsequently give rise to more easily identifiable and, therefore, more comparable structures and morphologies. **Figure 1** displays the top-view SEM and cross-section (S)TEM studies carried out on a vanadium zig-zag GLAD sample (t_{ON} = 0 s) before annealing. The characteristic surface microstructure of this porous GLAD film formed by associations of nanocolumns is highlighted in **Fig. 1(a)**. The layer thickness, as well as the zig-zag structures developed, are examined in **Fig. 1(b–c)**, which comprise TEM scans corresponding to regions around the center and the edge of the same sample, respectively. As can be seen here, the microstructure in both regions is slightly different. That is the central zone has similar nominal thicknesses for each of the sublayers t_1 (lower) and t_2 (upper), whereas close to the edge, it is fulfilled that $t_1 < t_2$. However, the overall thickness of the coating remains constant in either case. This demonstrates that the fabrication of zig-zag nanostructured coatings is a simple and effective solution to the problem of progressive wedging in GLAD monolayers. For a better insight into the generated zig-zag porous structures, **Fig. 1(d–f)** show the nanoscale STEM-EDX analyses carried out in a central region of this sample. **Fig. 1(e)** is a map where the X-ray net intensity (i.e. after background substraction) counts of vanadium associated to its main energy peaks are represented, whereas **Fig. 1(f)** is the EDX spectrum that can be extracted after summing all the signals within the region squared in the previous figures. It becomes clear that vanadium is the predominating element in this area, as expected from this system. On another note, it is observed that sublayer t_2 has a greater overall porosity in with respect to t_1. This can be explained by the fact that the tip of the taller nanocolumns in t_1 would serve as seeds for the proliferation of those eventually developed in t_2, resulting in a

growth regime that is exclusively dominated by shadowing events (i.e. higher porosity)[27,28].

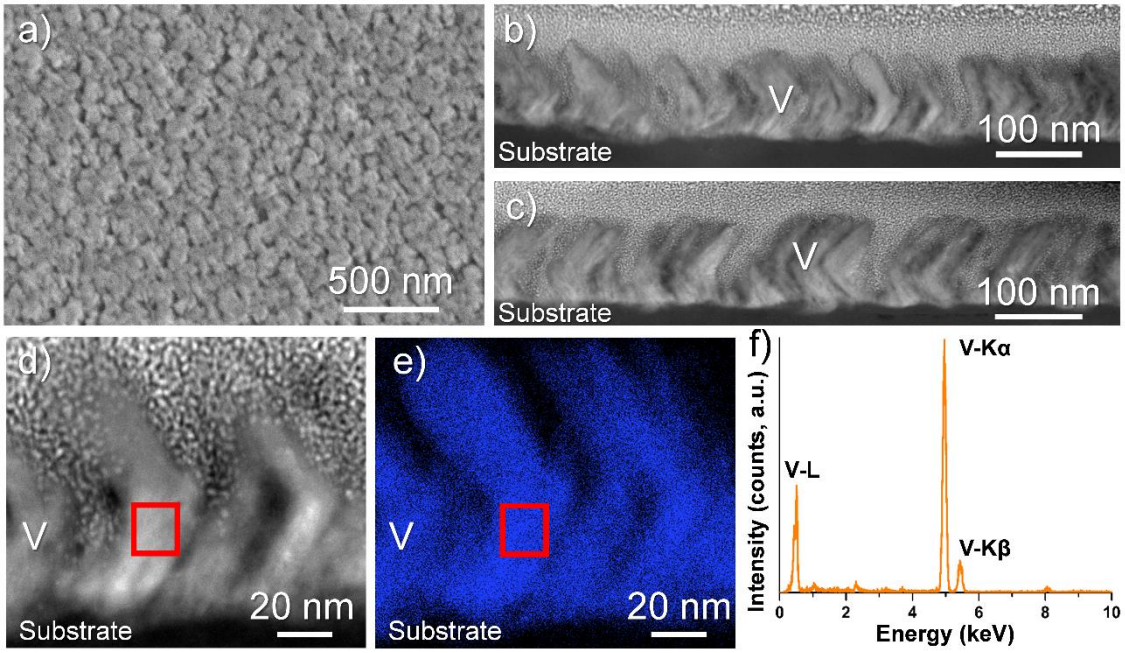

Figure 1. Electron microscopy analyses performed on a vanadium (t_{ON} = 0 s) zig-zag GLAD film of 100 nm nominal thickness. (a) Top-view SEM image. Cross-section bright-field (BF) TEM micrographs for (b) central and (c) edge regions within the sample. (d) Magnified BF-TEM micrograph of a region in (b) together with (e) the associated STEM-EDX net intensity map obtained for V atoms. (f) EDX integrated spectrum for the region defined by the red square in (d) and (e).

Figure 2 collects the GIXRD diffractograms obtained for 100 nm thick samples before and after annealing. As can be seen, the sample deposited in the absence of reactive oxygen presents a well-defined diffraction peak corresponding to metallic V (111) surfaces (JCPDS Card No. 01-085-4786). As t_{ON} increases, the crystallinity of the samples is weakened as a direct consequence of the increase in the average energy of the particles that reach the substrate[34]. Likewise, this increase in oxygen injection

times leads to decrease of intensity and shifts towards smaller angles of the observed diffraction peaks, which could be linked to the incorporation of O_2 into the cubic structure of vanadium. This may give rise to the formation of rather amorphous VO_{2-x} mixtures of undefined or complex stoichiometry such as $V_{16}O_3$ (JCPDS Card No. 04–011–0169). On the other hand, the diffractograms resulting from subjecting the previous samples to the same thermal treatment at 475ºC for 60 s (samples S100_475_1–3) disclose the formation of mixtures of VO_2(M) (JCPDS Card No. 03-65-2358) and a minority of V_2O_5 (JCPDS Card No. 00-041-1426), although with a decreasing intensity of the VO_2 (011) diffraction peak as t_{ON} increases. This leads to think that oxidation of samples with higher oxygen content may result in a detriment either in the VO_2 formation yield or, based on what was observed in the precursor films, in their crystallinity. The following studies with other characterization techniques help to find an explanation for this.

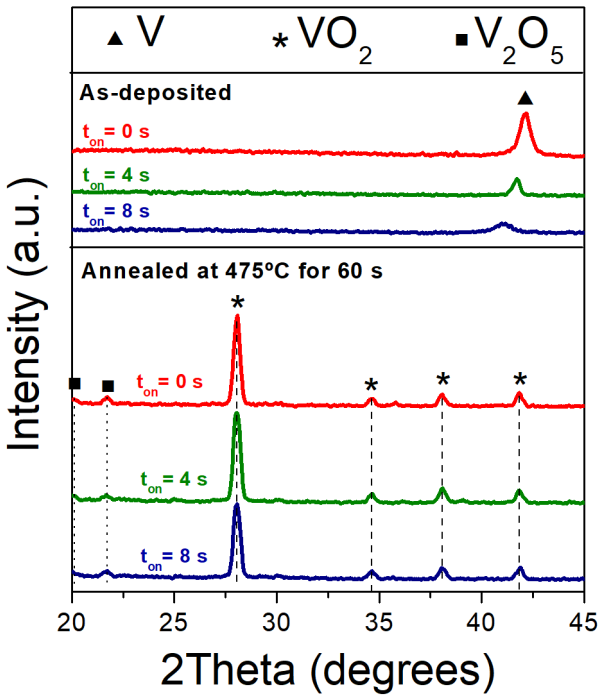

Figure 2. GIXRD diffractograms for 100 nm thick VO_{2-x} zig-zag GLAD samples deposited at oxygen injection times of 0 (red), 4 (green) and 8 s (blue) before and after annealing at 475ºC for 60 s, as labeled in the images.

Figure 3 shows the effect of oxygen injection times on the surface microstructures developed in samples rapidly annealed at 550ºC for 5 s. While sample S100_550_1 (**Fig. 3(a)**) exhibits a relatively homogeneous granular structure, increasing t_{ON} gives rise to the formation of progressively bigger grains but with more irregular morphologies (samples S100_550_2 and S100_550_3 displayed in **Fig. 3(b)** and **(c)**, respectively). In addition, there is a gradual formation of micro-rods-like structures randomly distributed in all directions, which is a characteristic feature of V_2O_5[38,39]. A similar trend also appears in samples S100_475_2 and S100_475_3 (to see the top-view SEM micrographs of these samples, refer to Supplementary Material Section I). Therefore, the intensity drops recorded in the above samples for the main VO_2(M) X-ray diffraction peaks at longer oxygen pulses would rather be related to an apparent rising of V_2O_5 yields, which consequently lowers those of the dioxide. This suggests a more favored air oxidation at higher t_{ON}, which in turn would also justify the development of globally larger microstructures at the cost of increasingly heterogeneous morphologies and grain size distributions.

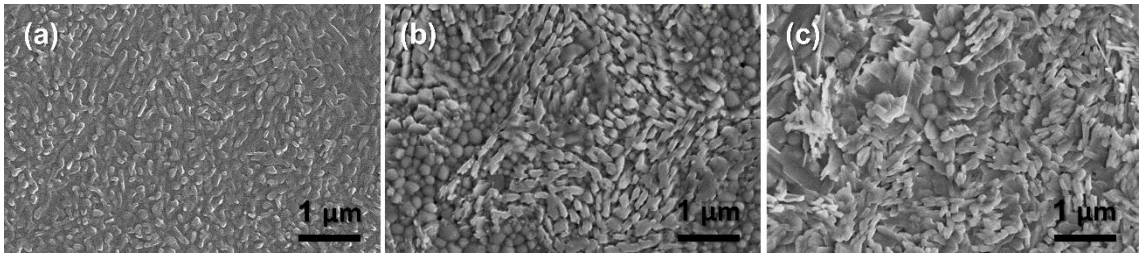

Figure 3. SEM micrographs depicting the surface topography of samples (a) S100_550_1, (b) S100_550_2, and (c) S100_550_3.

In order to address a more in-depth characterization, S100_550_1–3 samples were prepared for their observation at the nanoscale by (S)TEM techniques. **Figure 4** displays the main results of the BF-TEM and HRTEM examinations carried out on the previous samples. These figures reveal once again that there is a progressive and simultaneous increase of both the average grain size and the heterogeneity of the synthesized films as for longer t_{ON}. This also leads to a lower compactness of the film and thus the appearance of loose grain boundaries throughout the treated layer (see **Fig. 4(a–c)**). This feature could somehow promote a progressively higher overall porosity of the coating that entails positive consequences from the perspective of their optical behavior (i.e. greater transmittance). Interestingly, and besides these variations, the HRTEM analyses of these coatings at the regions indicated in **Fig. 4(a–c)**, which are magnified in **Fig. 4(d–f)**, evidenced the successful synthesis of VO_2(M) regardless of the absence or duration of the oxygen pulses used during the deposition process. This hypothesis is proved when the Fast Fourier Transformed (FFT) of the regions imaged is retrieved and measured in each one of these local areas. By studying these arrangements of spots in both the direct (i.e. by checking the lattice planes present between consecutive rows of atomic columns) and the reciprocal space (i.e. by measuring the angles between the brightest spots, related to the aforementioned lattice planes) it is possible to eventually determine that the resulting values match best with intensity distributions that are generated by VO_2 crystals when they are observed along three different zone axes: [120] (**Fig. 4(d)**), [100] (**Fig. 4(e)**) and [122] (**Fig. 4(f)**).

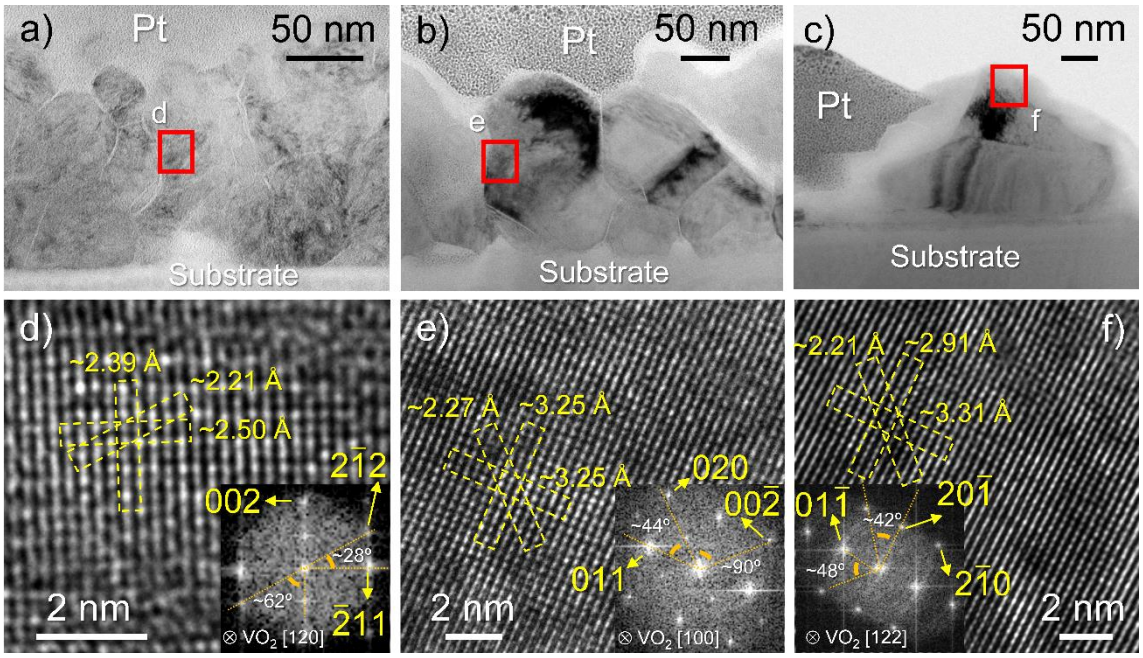

Figure 4. Summary of the TEM studies performed on samples S100_550_1–3. Bright-field (BF) TEM overview of samples (a) S100_550_1, (b) S100_550_2 and (c) S100_550_3. (d–f) HRTEM micrographs of the narrow regions highlighted in (a–c) together with their associated FFT spectra.

For a better understanding on how oxidation occurs as well as to identify the vanadium oxides synthesized throughout the film thickness for different values of t_{ON}, **Figure 5** illustrates the analytical (S)TEM-EELS studies performed on samples S100_550_1–3. As advanced in the experimental section, and as done in previous works[34,40], the spectra were registered at an energy range where both the V-$L_{2,3}$ white lines, the O-K pre-edge region and the t_{2g} and e_g states. By studying the energy positions of these

signals as well as their intensities or just their actual presence, it is possible to qualitatively determine the presence of vanadium oxides of specific oxidation states. The spectra are represented by gathering and processing all the signals detected in the regions within the rectangles of the same colors. This allows to determine the oxidation state of the coatings at different distances from the substrate. Almost all the cases suggest the presence of vanadium dioxide (VO_2) because the following features are found simultaneously[41,42]: (i) the separation between V-$L_{2,3}$ white lines is lower than that in metallic vanadium (i.e. below 7 eV); (ii) these lines exhibit weak shoulders at their left side (note them most clearly in **Fig. 5(f–g)**); and (iii) both the t_{2g} and e_g peaks appear and the former has a higher intensity than the latter. The only exception in this trend is the pink-colored spectrum in **Fig. 5(g)**, where the positions and intensities of these four peaks rather lead to the presence of vanadium pentoxide (V_2O_5) at regions closer to the surface[41,43]. This suggests that the oxidation is more aggressive at these regions because of the easier exposure to oxygen, which is further eased in sample S100_550_3 thanks to the higher t_{ON} chosen for this sample.

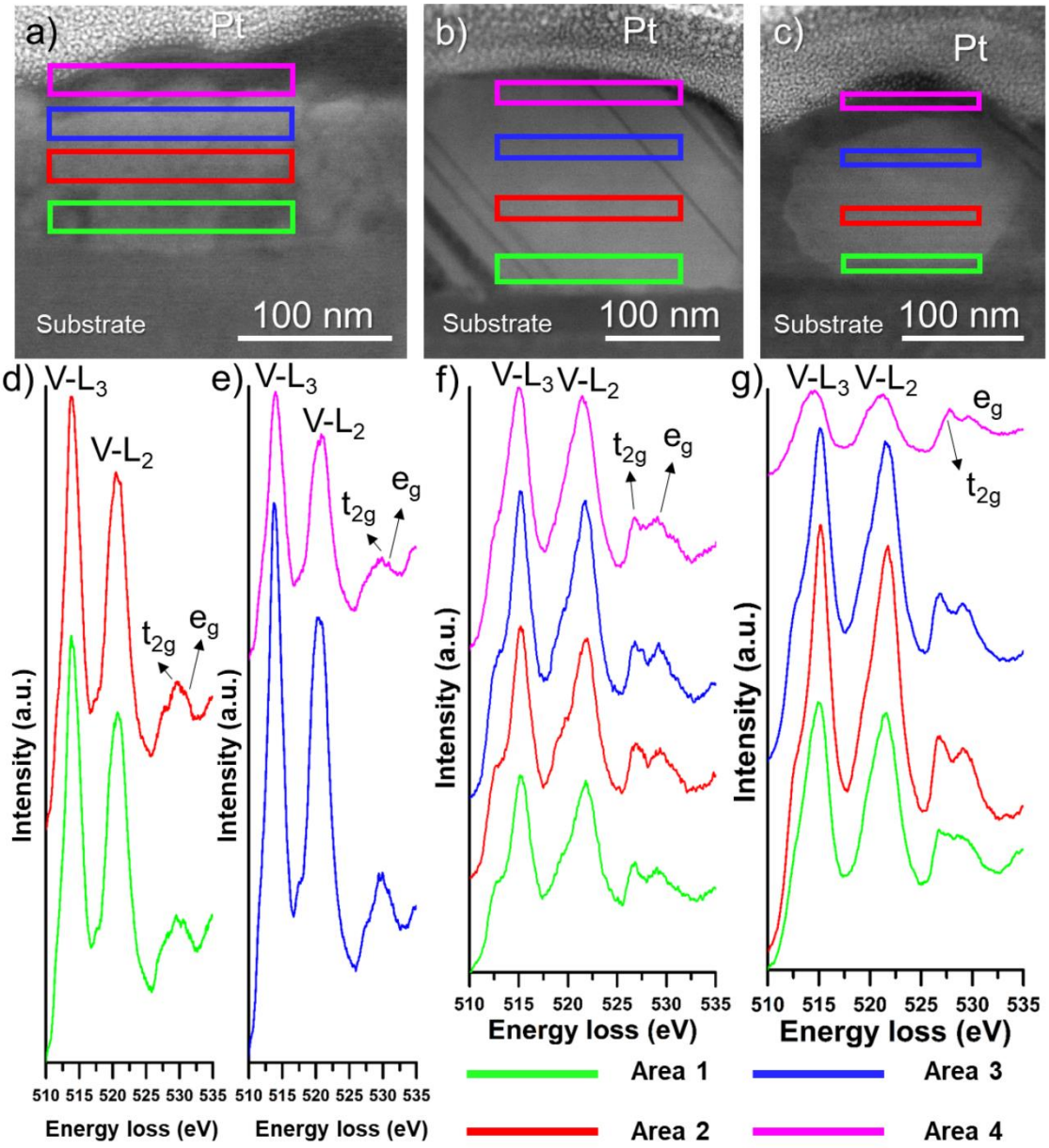

Figure 5. STEM-EELS analysis performed on samples S100_550_1–3. High-angle annular dark-field (HAADF) overviews of samples (a) S100_550_1, (b) S100_550_2, (c) S100_550_3. (d–g) Integrated EELS spectra corresponding to the areas marked in (a–c).

Based on the outcomes achieved so far, it can be preliminarily concluded that the atmospheric oxidation of VO_{2-x} zig-zag GLAD films succeeds in the synthesis of films

that are mainly composed of VO_2(M), with larger and morphologically more heterogeneous grains as t_{ON} increases. It has also been disclosed that this oxidation evolves from the surface towards the interface with the substrate, hence the surface formation of V_2O_5 observed in several samples that is more accentuated for longer oxygen injection times. However, this latter feature would not be a disadvantage, but rather the opposite, since it has been proven that V_2O_5 can act as a protective layer for VO_2 against external agents such as air or humidity, thus enhancing the durability of the coating[44,45].

3.2. Optical characterization

In order to evaluate the optical thermochromic response of the fabricated coatings and, in particular, the parameters that define their viability for application in smart windows, Vis-NIR transmittance measurements (at wavelength ranges between 350 and 2500 nm) were carried out at 25 and 90ºC for all the samples addressed in the present study. The values of the photometric (T_{lum}) and radiometric (T_{sol}, T_{IR}) parameters calculated from these results are shown in **Table 2**. The study of the kinetic evolution of transmittance at 2000 nm for successive heating-cooling cycles between 25–90ºC at constant rates was also performed to record the features of the reversible MIT hysteresis loops. The transition temperatures for heating ($T_{c(H)}$) and cooling ($T_{c(C)}$) cycles, calculated from the derivative curves of the transmittance *vs.* temperature plots with Gaussian fits, and the resulting hysteresis widths (W_H) are listed in **Table 3**.

Table 2. Radiometric and photometric parameters changes with heating for all the studied samples. For a detailed definition and explanation about how all these parameters are obtained, refer to the work of Outón *et al.* (Appendix A)[16]. The accuracy of these values is ±0.1%.

Sample	T_{lum} (%)	ΔT_{lum} (%)	ΔT_{sol} (%)	$\Delta T_{sol.\ rel}$ (%)	ΔT_{IR} (%)	$\Delta T_{IR.\ rel}$ (%)
S100_475_1	17.7	4.0	8.0	41.1	13.7	58.3
S100_475_2	18.0	4.4	12.0	50.1	23.0	69.1
S100_475_3	26.7	3.3	9.8	31.6	18.4	46.9
S100_550_1	15.7	4.3	10.7	52.3	19.4	71.7
S100_550_2	16.2	1.2	10.7	45.5	22.8	66.2
S100_550_3	8.1	-2.8	1.4	9.1	6.8	26.9
S50_475_1	40.1	3.2	5.5	16.2	10.1	28.3
S50_475_2	48.7	4.7	4.8	11.0	7.7	16.0
S50_475_3	46.9	6.1	6.9	16.5	10.1	22.0
S50_550_1	45.6	0.3	4.2	10.0	9.8	21.4
S50_550_2	40.3	5.2	7.5	20.7	13.6	33.7
S50_550_3	54.0	1.2	2.8	5.6	5.8	10.7
S25_500_1	46.2	-0.9	3.3	6.9	9.0	16.6
S25_500_2	52.7	-0.9	3.2	6.2	8.5	15.1
S25_500_3	55.6	1.1	4.8	8.5	9.6	15.1

Figure 6 displays the results obtained from the optical characterization of 100 nm thick zig-zag GLAD samples. Overall, it can be seen that the oxidation of zig-zag nanostructures deposited at t_{ON} = 0 s gives rise to optical responses comparable, especially in terms of NIR transmittance drops, to those previously reported for single-layer V-GLAD systems[26], demonstrating once again the validity of this new approach. Focusing initially on the samples oxidized at 475°C for 60 s, a progressive enhancement of the visible transmittance can be observed with t_{ON} (**Fig. 6(a)**). This would reinforce the previous assumption about the apparent gradual increase in overall porosity as a consequence of the microstructural changes induced by the formation of other vanadium oxides. In this sense, and in agreement with what was previously evidenced by XRD and SEM, the presence of maximum transmittance peaks at ~600

nm (higher in sample S100_475_3) denotes the presence of V_2O_5 in all these samples. Notwithstanding, it seems that this compound does not have a very significant detrimental effect on the solar modulation ability of the coating (ΔT_{sol} = 9.8% for S100_475_3, compared to 8.0 and 12.0% achieved for t_{ON} = 0 and 4 s, respectively). Equally striking are the ΔT_{lum} values calculated for all these samples (between 3.3–4.4%), which contribute to a greater ΔT_{sol} (solar radiation of higher intensity in the visible range). In previous works[25,26], this event was somehow associated with the development of VO_2 + VO_{2+x} mixtures, although its origin remains unclear. Apart from that, the values of $\Delta T_{IR, rel}$, which can be considered as indirect indicators/comparators of the VO_2 yields attained, suggest a higher VO_2 content for sample S100_475_2.

Table 3. Main features of the thermochromic hysteresis loops of all the studied samples. $T_{c(H1)}$ and $T_{c(H2)}$ denote the temperatures of the MIT transition on heating; $T_{c(C1)}$ and $T_{c(C2)}$ indicate the temperatures of the MIT transition on cooling; and W_{H1} and W_{H2} are the hysteresis loop widths given by $T_{c(H1)} - T_{c(C1)}$ and $T_{c(H2)} - T_{c(C2)}$, respectively. The accuracy of the temperature values is ±0.5ºC.

Sample	**T_c (ºC) heating**		**T_c (ºC) cooling**		**W_H (ºC)**	
	H1	**H2**	**C1**	**C2**	**1**	**2**
S100_475_1	62	70*	48	58*	14	12
S100_475_2	73*	77	60*	42	13	35
S100_475_3	78*	85	65*	44	13	41
S100_550_1	68	73*	52	62*	16	11
S100_550_2	69*	74	61*	43	8	31
S100_550_3	71*	78	60*	41	11	37
S50_475_1	56	75*	52		4	23
S50_475_2	79*	87	61*	45	18	42
S50_475_3	66*	69	41*	53	25	16
S50_550_1	57	63*	45		12	18
S50_550_2	70*	82	50		20	32
S50_550_3	62*	65	43*	45	19	20
S25_500_1	57*	68	40*	48	17	20
S25_500_2	69		48		21	
S25_500_3	61*	69	43		18	26

* Main peak

On the other hand, the rapid annealing carried out at 550 °C for 5 s for 100 nm thick samples entails considerably different behaviors (**Fig. 6(b)**). While the samples deposited at t_{ON} = 0 and 4 s show similar trends to those previously observed (i.e. higher T_{lum} and ΔT_{IR} at longer t_{ON}), the solar modulation ability of the sample S100_550_3 is severely compromised (ΔT_{sol} = 1.4%). This is a consequence of the shift of the intersection between the low and high temperature spectra towards longer wavelengths, which in turn translates into negative ΔT_{lum} values. Moreover, the light transmittance of this sample is abnormally low, which breaks with previously observed tendencies. Spectra similar to the above have been found in the literature[46–49]. Although no

specific reason for this feature has been found so far, everything seems to indicate that it could have its origin in the joint action of a porosity manifested as large intergranular voids and an inhomogeneous distribution of the synthesized grains forming agglomerations. This hypothesis would also be supported by the findings by SEM and TEM previously presented. In this sense, it can be ruled out that this phenomenon is directly related to the presence of V_2O_5, given the absence of such characteristics in the spectra collected in **Fig. 6(a)** (i.e. VO_2 + V_2O_5 mixtures). It is therefore clear that, even if considerable VO_2 yields are reached, the size, morphology and arrangement of the synthesized structures play a direct and key role on the T_{lum} and ΔT_{sol} values of the coating. Likewise, it is worth noting that the ΔT_{sol} values reported for t_{ON} = 0 and 4 s are very good (10.7% for both samples), with slightly higher VO_2 yields for the S100_550_0 sample according to the $\Delta T_{IR,rel}$ values. However, the insufficient T_{lum} values accomplished for all 100 nm thick samples make their application in smart windows unfeasible.

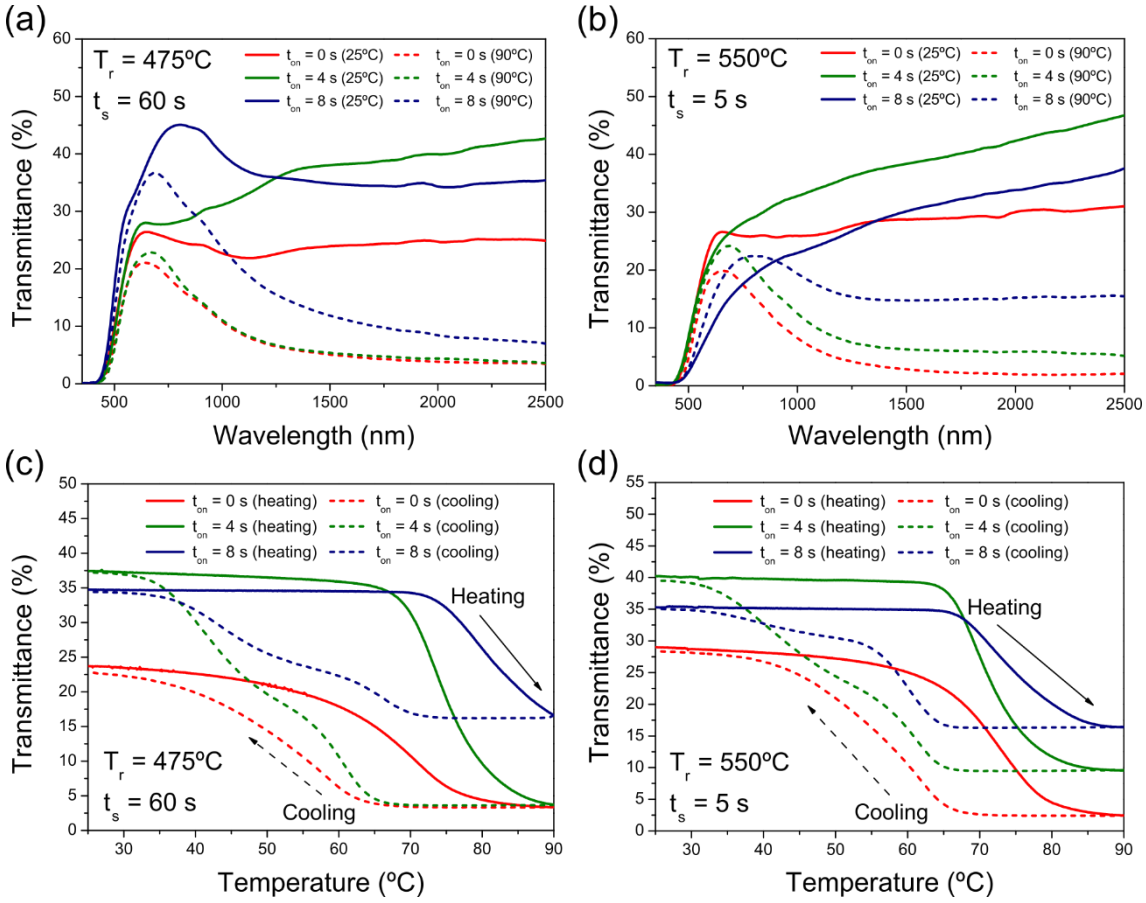

Figure 6. Vis-NIR optical measurements performed on 100 nm thick VO_{2-x} zig-zag GLAD annealed samples. Transmittance spectra recorded at 25 °C (solid lines) and 90 °C (dashed lines) for samples thermally treated at (a) 475 °C for 60 s, and (b) 550 °C for 5 s. Thermal evolution of the optical transmittance at 2000 nm recorded during consecutive heating (solid lines) and cooling (dashed lines) cycles for samples thermally treated at (c) 475 °C for 60 s, and (d) 550 °C for 5 s.

Fig. 6(c–d) reveals the features of the resulting hysteresis loops for each one of the aforementioned samples. In general terms, it can be clearly observed how longer oxygen pulses give rise to gradual and simultaneous increases in T_c and W_H. This also leads to the appearance of increasingly asymmetric hysteresis, becoming especially visible during the cooling stage. The derivative curves for each thermochromic kinetic cycle

(see Figure S2 in Supplementary Material Section II) disclose the development of two-step transitions. This translates into the existence of two critical temperatures (two different slopes) for each heating and cooling stage, as well as variable hysteresis widths (see **Table 3**). It should be clarified here that, while the assignment criteria for H1 and H2 are based exclusively on rising temperatures, the nomenclatures for C1 and C2 are imposed on the basis of the analogies found between the heating-cooling stages (e.g. peaks with equivalent variation rates, full width at half maximum or FWHM, ...). Thus, while some of these asymmetries are somewhat hidden due to the overlapping of the two minimum variation peaks (e.g. samples S100_475_1 and S100_550_1), others become more evident as a consequence of their splitting. This asymmetry in hysteresis was previously observed for rapid atmospheric oxidation of V-GLAD films, and related to the presence of VO_2 crystalline grains of different sizes[50]. On that occasion, however, neither such wide hysteresis nor high T_c were reported, but quite the opposite[26].

First, there is no clear reason to think that both W_H and T_c increases can be directly attributed to the presence of V_2O_5, since, for instance, sample S100_550_2, consisting mainly of VO_2(M), also exhibits these characteristics. According to the literature, broader hysteresis occurs with increasing particle size[51], as well as by the presence of loose grain boundaries (i.e. not entirely connected to adjacent ones), thus limiting the propagation of the metal-to-insulator transition[47]. This is in good agreement with the SEM and TEM micrographs. On the other hand, explaining the increase in T_c with t_{ON} is more complex. It has been reported that this may be due either to residual stress along the *c*-axis of VO_2[52], or to the adsorption of oxygen atoms[53]. The latter would partially explain what has been observed for samples deposited at longer oxygen pulses. However, another previous work reported that the oxidation of VO_{2-x} GLAD films on

Si substrates led to the occurrence of increasing residual stress for longer t_{ON}, even resulting in the development of large cracks in the films[34]. So either of these two phenomena could serve as an explanation for the increases in T_c observed here.

In short, it has been evidenced that the oxidation of 100 nm GLAD VO_{2-x} zig-zag samples leads to really good solar modulation abilities, especially for samples deposited with t_{ON} = 4 s (ΔT_{sol} = 10.7–12.0 %). Furthermore, longer oxygen injection pulses give rise to simultaneous and substantial increases in W_H (variable maximum hysteresis width of 13–41°C for sample S100_475_3) and, except as observed for sample S100_550_3, in luminous transmittance, although with values still far below (T_{lum} < 27%) those required for smart window applications. Likewise, greater t_{ON} also drives to considerable and progressive increases in T_c, which is a major drawback. However, the outstanding ΔT_{sol} and W_H values reported for most of these samples make them suitable for application in optical storage-type devices[47,54].

Nevertheless, the optical behavior of these systems also depends on the thickness of the coating. **Figure 7** shows how by reducing the layer thickness down to 50 nm and increasing the duration of the oxygen pulses, considerably higher T_{lum} performances (> 46%) can be achieved, although at the expense of ΔT_{sol} (see **Table 2**). In fine agreement with what was previously observed for the 100 nm thick samples, increasingly asymmetric hysteresis continues to develop as t_{ON} increases (see Figure S3 in Supplementary Material section II). However, on this occasion the samples deposited at t_{ON} = 4 s are the ones that present the broadest hysteresis (maximum W_H = 32–42ºC), although still with $T_{c(H)}$ above the standard value reported for pure VO_2(M) (~68ºC). On the contrary, the samples deposited at t_{ON} = 8 s also give rise to wide hysteresis (always above 16ºC), although with critical temperatures between 62–66ºC during heating, which, in addition to breaking with the trends seen above, represents a substantial

improvement over the values achieved for 100 nm thick samples. In general, it is well known that lowering thicknesses leads to drops in critical temperatures as a result of increases in residual tensile stress near the film-substrate interface[44,55,56]. It has also been evidenced that flash annealing favors the development of oxygen-deficiency-related defects[57], which in turn translates into considerable drops in T_c. This explains the lower critical temperatures attained for samples annealed instantaneously at 550ºC compared to those obtained at 475ºC for 60 s reaction times.

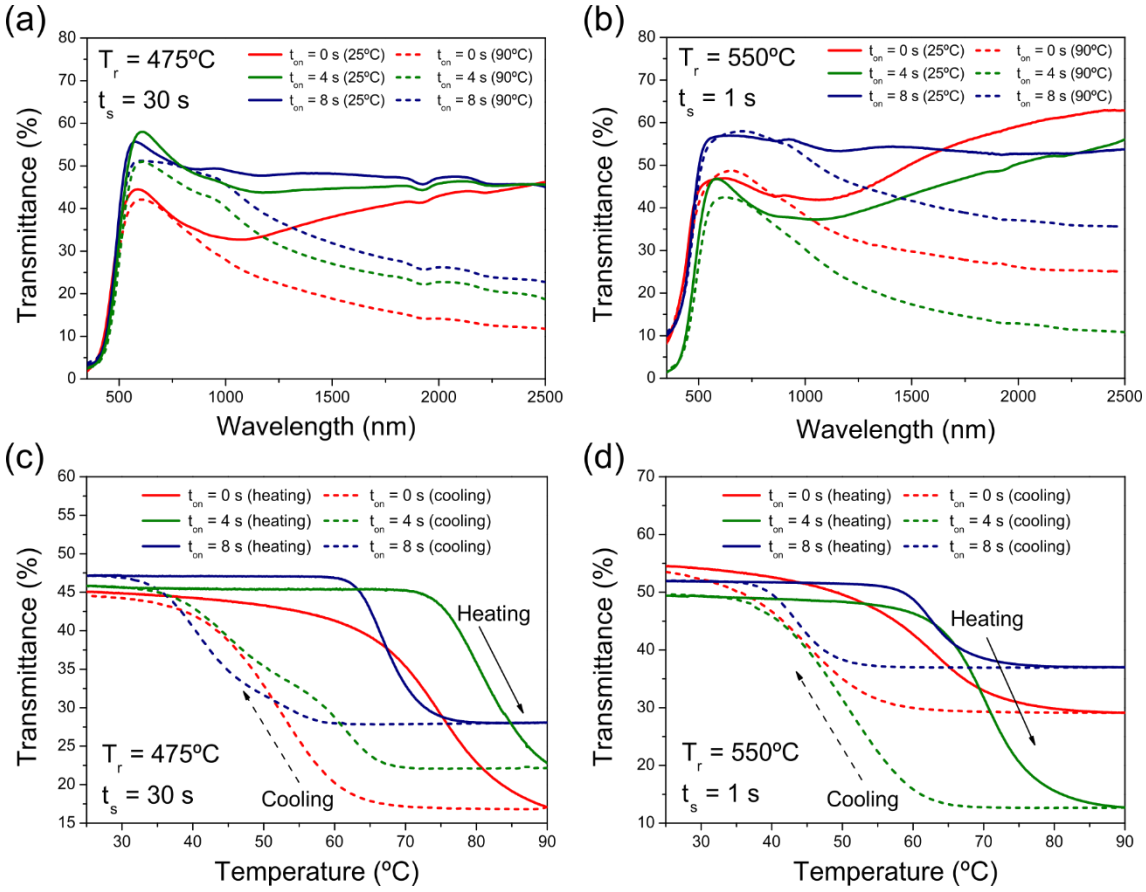

Figure 7. Vis-NIR optical measurements performed on 50 nm thick VO_{2-x} zig-zag GLAD annealed samples. Transmittance spectra recorded at 25 °C (solid lines) and 90 °C (dashed lines) for samples thermally treated at (a) 475 °C for 30 s, and (b) 550 °C for 1 s. Thermal evolution of the optical transmittance at 2000 nm recorded during consecutive heating (solid lines) and cooling (dashed lines) cycles for samples thermally treated at (c) 475 °C for 30 s, and (d) 550 °C for 1 s.

On the other hand, it is still necessary to find an explanation for the drop in critical temperatures of the samples deposited at t_{ON} = 8 s. At this point of the work, it is clear that the increases in W_H and T_c are interrelated, leading to think that both are due to purely microstructural issues (e.g. grain size and heterogeneity, loose grain boundaries). As previously observed[34], the deposition of VO_{2-x} films by GLAD + RGPP

approaches results in the development of films of distinct nature (morphology, degree of compaction) as a consequence of different deposition dynamics. From these studies, it can be assumed that the threshold thickness at which GLAD deposition starts to be driven by shadowing effects is greater for t_{ON} = 8 s. Thus, unlike the features observed in VO_{2-x} films fabricated with shorter oxygen pulses, GLAD deposition at t_{ON} = 8 s would be mainly governed by diffusive phenomena when the nominal layer thickness is below 50 nm. Although this results in lower overall porosities, it would allow the synthesis of more homogeneous surface microstructures before and after thermal treatments, with the reduction of reactivity (due to the lowered surface-to-volume ratios) being compensated by an increase of the oxygen concentration inside the film. Hence the formation of relatively large grains, which would explain the occurrence of wide hysteresis. In this framework, it is worth highlighting the good results obtained for sample S50_475_3, which not only exhibits a fairly good balance of T_{lum} and ΔT_{sol} (46.9% and 6.9%, respectively), but also a main $T_{c(H)}$ of 66ºC and a variable W_H of between 16–25ºC, which at the same time makes it suitable (together with sample S50_550_2; ΔT_{sol} = 7.5% and W_H = 20–32ºC) for application in optical memory devices.

Finally, **Figure 8** illustrates the outcomes derived from the optical characterization of 25 nm thick zig-zag GLAD samples after flash annealing at 500ºC. In general terms, the tendencies observed for 50 nm thick samples are maintained, although in these cases, the development of hysteresis asymmetries is not so evident (for a more detailed overview on this, refer to Fig. S4 in Supplementary Material Section II). Thinner films imply instantaneous thermal treatments at lower temperatures, favoring the formation of smaller and more homogeneous grains. Such thicknesses also lead to diffusion-dominated GLAD deposition regimens regardless of t_{ON} (i.e. the thickness is so narrow

that the threshold at which shadowing events start to occur is not exceeded). This, in turn, would support our previous hypotheses about the development of increasingly wider hysteresis with t_{ON} (i.e. by increasing grain size) at similar porosity levels. Furthermore, the $\Delta T_{IR,rel}$ values achieved for all these samples suggest similar VO_2(M) yields.

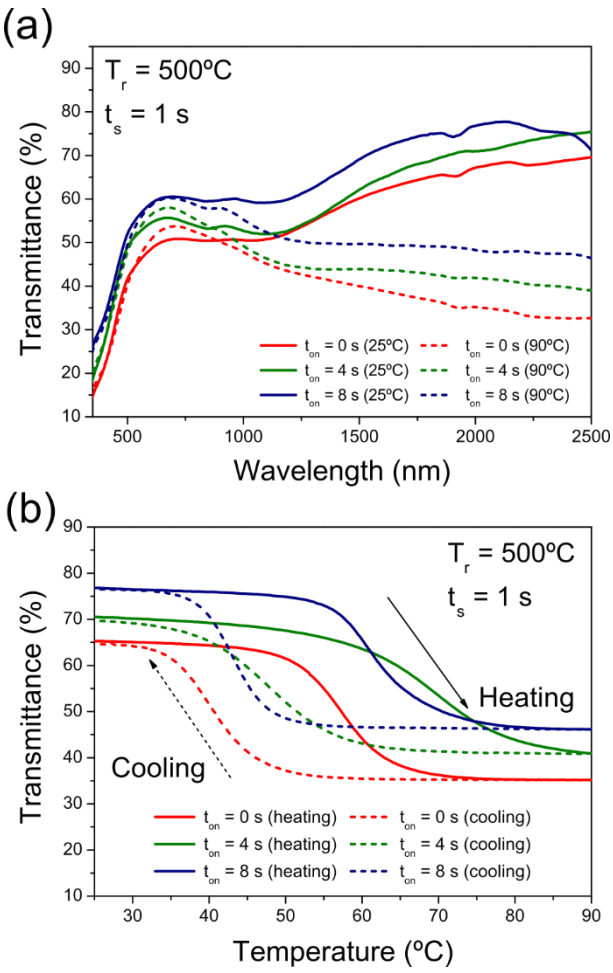

Figure 8. Vis-NIR optical measurements performed on 25 nm thick VO_{2-x} zig-zag GLAD samples instantaneously annealed at 500ºC. (a) Transmittance spectra recorded at 25 °C (solid lines) and 90 °C (dashed lines). (b) Thermal evolution of the optical transmittance at 2000 nm recorded during consecutive heating (solid lines) and cooling (dashed lines) cycles.

Conversely, lower layer thicknesses not only lead to even higher T_{lum} values, but also to lower T_c, although again with more pronounced detriments of ΔT_{sol}. In any case, it is worth highlighting the good results obtained for t_{ON} = 8 s, with remarkable balances of T_{lum} (55.6%) and ΔT_{sol} (4.8%) for sample S25_500_3, accompanied by beneficial decreases in $T_{c(H)}$ up to 7ºC below the 68ºC reported for pure VO_2(M) and outstanding variable hysteresis widths of 18–26ºC. These results are undoubtedly a considerable improvement over those obtained by rapid and air oxidation of V-GLAD monolayers[25,26], especially in terms of T_{lum} and W_H, while facing the problem inherent to this deposition variant that promotes the development of inhomogeneous layer thicknesses. Moreover, these performances are even more noteworthy if the negative effects coming from the glass substrate are neglected and only the film parameters are taken into account, resulting in T_{lum} and ΔT_{sol} relationships of 67.8% and 5.7%, respectively (see Supplementary Material Section III). All of the above makes this sample potentially interesting for smart window applications, albeit it would still require a further lowering in MIT temperatures through elemental doping strategies, which are currently planned as prospective work.

3.3. Electrical characterization

In order to explore additional applications for the 100 nm thick annealed samples, DC electrical resistivity *vs.* temperature measurements were carried out between 25–90ºC. The results obtained are collected in **Figure 9** and **Table 4**. The transition temperatures (T_c) during heating and cooling cycles were calculated from the derivative curves of the resistivity *vs*. temperature plots (**Fig. 9**) by fitting them with a Gaussian function and considering the resulting peaks as the temperatures of the minima variation rates. The hysteresis loop widths (W_H) given by T_c(heating) – T_c(cooling), the ratio of resistivities

at 25ºC and 90ºC, and the order of magnitude of the resistivity drop, calculated through the common logarithm of these ratios, are also reported. In contrast to the optical characterization, the oxidized vanadium samples (t_{ON} = 0 s) show symmetrical and relatively narrow electrical hysteresis (W_H = 8ºC). Besides, longer t_{ON} leads to progressive increases in $T_{c(H)}$ (although not as high as those reported by the transmittance *vs.* temperature measurements) and in W_H, this latter accompanied by the development of asymmetric hysteresis during the cooling stage. All of the above highlights, once again, the different driving forces of optical and structural MITs, the latter having been associated rather with electrical changes in VO_2(M) systems[40].

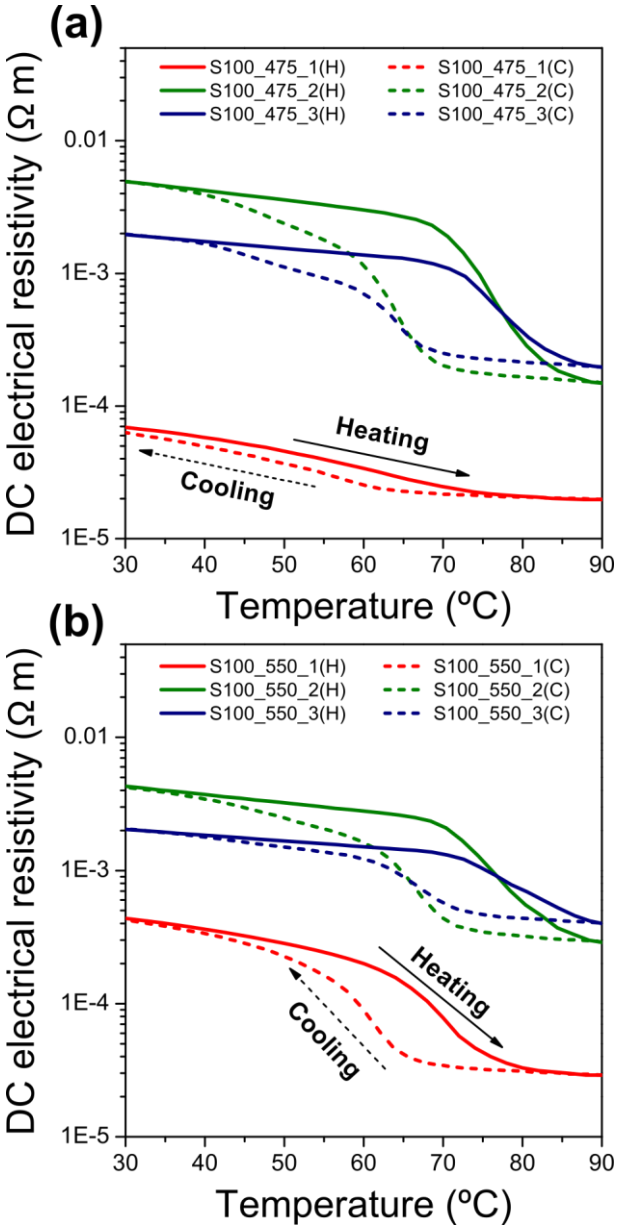

Figure 9. Changes in electrical resistivity with temperature for 100 nm thick VO_{2-x} zig-zag GLAD samples annealed at (a) 475ºC for 60 s and (b) 550ºC for 5 s registered during consecutive heating (solid lines) and cooling (dashed lines) cycles.

Taking into account the fast nature of the thermal treatments addressed as well as the limitation that this may imply in terms of size and crystallinity of the synthesized VO_2(M) grains, it can be considered that the results achieved in this section are

relatively positive. The oxidation of samples deposited at longer oxygen pulses promotes the generation of larger crystallites, which results in lower grain boundary densities and, therefore, of intergranular barriers hindering the movement of electrons. In this sense, it is worth mentioning the more limited resistivity drops for t_{ON} = 8 s samples, particularly for sample S100_550_3, which could be closely related to the presence of the large voids (previously observed by SEM and TEM studies) acting as additional electronic barriers. The results above make the samples deposited at t_{ON} = 4 s the most interesting from an electrical point of view, since they register resistivity drops of 1.2–1.6 orders of magnitude. This not only represents a substantial improvement over those achieved by means of the oxidation of single-layer V-GLAD films of similar thickness[26], but also enables the alternative application of these systems in a multitude of simultaneous electro-optical phase change devices[58].

Table 4. Main electronic features of the MIT extracted from the resistivity *vs.* temperature measurements carried out on samples S100_475_1–3 and S100_550_1–3. The accuracies of temperature and resistivity values are ±0.5 °C and $\pm 10^{-6}$ Ω m, respectively.

Sample	T_c (ºC) heating	T_c (ºC) cooling	W_H (ºC)	ρ(25ºC)/ρ(90ºC)	Order of Magnitude
S100_475_1	64	56	8	3.8	~ 0.6
S100_475_2	72	65/45	7/27	37.3	~ 1.6
S100_475_3	75	63/44	12/31	12.0	~ 1
S100_550_1	67	59	8	16.6	~ 1.2
S100_550_2	72	64/44	8/28	16.6	~ 1.2
S100_550_3	75	65/41	10/34	5.4	~ 0.7

4. Conclusions

It has been demonstrated that rapid and highly controlled air oxidation of zig-zag VO_{2-x} GLAD films of 25, 50 and 100 nm of homogeneous nominal thickness gives rise to the fabrication of VO_2-based coatings with microstructural characteristics strongly influenced by the duration of oxygen pulses used during the deposition processes. The size, morphology and arrangement of these microstructures have a determining effect on the optical and electrical thermochromic properties of coatings. Some of these events have a specific impact on one or several key parameters, although, in most cases, they take place to the detriment of other ones, making them more or less suitable for a given application. In this sense, it was evidenced that, regardless of the layer thickness, greater t_{ON} leads to simultaneous improvements in luminous transmittance and hysteresis width as a consequence of the formation of generally larger grains, although with heterogeneous morphology and grain size distributions. This means that the grains formed do not fit perfectly together, leaving gaps between them and somehow increasing the overall porosity of the coating. However, this leads to undesired increases in T_c as well as the development of asymmetric hysteresis loops. Despite the excellent ΔT_{sol} values attained for 100 nm thick samples, the insufficient T_{lum} (< 27%) and abnormally high $T_{c(H)}$ (> 68°C) values recorded for longer oxygen pulses make them rather suitable for application in optical-electronic phase-change devices (given the acceptable electrical properties evidenced in samples deposited at t_{ON} = 4 s) or in optical storage-type systems (maximum variable hysteresis widths up to 41°C for higher t_{ON}).

In contrast, 25 and 50 nm thick samples deposited at t_{ON} = 8 s give rise to similarly broad hysteresis ($W_H \geq 16$ºC), although with MIT temperatures during heating 2–7ºC below the ordinary value reported for pure VO_2(M) films (~68ºC). The latter is explained by a vanadium GLAD deposition regime for t_{ON} = 8 s and layer thicknesses ≤

50 nm governed exclusively by diffusion events, favoring the homogeneity of the synthesized grain sizes. This allows the S25_500_3 sample to achieve optimal performances for smart glazing application, with T_{lum} and ΔT_{sol} values above 55% and 5%, respectively, coupled with beneficial $T_{c(H)}$ drops without doping and extraordinarily wide variable hysteresis (W_H =18–26ºC), representing a remarkable enhancement over what was previously accomplished through air oxidation of V-GLAD films. These investigations not only open up an alternative avenue for improvement towards the development of simple and cost-effective strategies for large-scale manufacturing of VO_2-based coatings, but also clear the horizon for addressing future doping as the next steps in this research line.

Acknowledgements

A. J. Santos would like to thank the University of Cádiz and the Spanish Ministerio de Universidades for the concession of a "Margarita Salas" postdoctoral fellowship funded by the European Union - NextGenerationEU (2021-067#9663/PN/MS-RECUAL/CD). University of Cádiz and IMEYMAT are also acknowledged by financing the mutual facilities available at the UCA R&D Central Services (SC-ICYT), the UCA project reference "PUENTE PR2022-027", and the IMEYMAT project reference "LÍNEAS PRIORITARIAS PLP2021120-1". This work was supported by the Spanish State R&D project (Retos y Generación de Conocimiento) ref. PID2020–114418RBI00. J. J. Jiménez and F. M. Morales acknowledge "Fondo Social Europeo y la Consejería de Transformación Económica, Industria, Conocimiento y Universidades" of this same institution (2021-001/PAI/PAIDI2020/CD). This work was partly supported by the French RENATECH network, FEMTO-ST technological facility, by the Region

Bourgogne-Franche-Comté and by EIPHI Graduate School (Contract “ANR–17–EURE–0002”).

Data availability statement

Data will be made available on request.

Declaration of Competing Interest

The authors declare that they have no known competing financial interests or personal relationships that could have appeared to influence the work reported in this paper.

REFERENCES

[1] B.N. Silva, M. Khan, K. Han, Towards sustainable smart cities: A review of trends, architectures, components, and open challenges in smart cities, Sustain. Cities Soc. 38 (2018) 697–713. doi:10.1016/j.scs.2018.01.053.

[2] K. Khaled, U. Berardi, Current and future coating technologies for architectural glazing applications, Energy Build. 244 (2021) 111022. doi:10.1016/j.enbuild.2021.111022.

[3] Y. Cui, Y. Ke, C. Liu, Z. Chen, N. Wang, L. Zhang, Y. Zhou, S. Wang, Y. Gao, Y. Long, Thermochromic VO_2 for energy-efficient smart windows, Joule. 2 (2018) 1707–1746. doi:10.1016/j.joule.2018.06.018.

[4] N. Shen, S. Chen, R. Huang, J. Huang, J. Li, R. Shi, S. Niu, A. Amini, C. Cheng, Vanadium dioxide for thermochromic smart windows in ambient conditions, Mater. Today Energy. 21 (2021) 100827. doi:10.1016/j.mtener.2021.100827.

[5] X. Cao, T. Chang, Z. Shao, F. Xu, H. Luo, P. Jin, Challenges and opportunities toward real application of VO_2-based smart glazing, Matter. 2 (2020) 862–881. doi:10.1016/j.matt.2020.02.009.

[6] S. Wang, T. Jiang, Y. Meng, R. Yang, G. Tan, Y. Long, Scalable thermochromic smart windows with passive radiative cooling regulation, Science. 374 (2021) 1501–1504. doi:10.1126/science.abg0291.

[7] X. Li, C. Cao, C. Liu, W. He, K. Wu, Y. Wang, B. Xu, Z. Tian, E. Song, J. Cui, G. Huang, C. Zheng, Z. Di, X. Cao, Y. Mei, Self-rolling of vanadium dioxide nanomembranes for enhanced multi-level solar modulation, Nat. Commun. 13 (2022) 7819. doi:10.1038/s41467-022-35513-w.

[8] J.-P. Pouget, Basic aspects of the metal–insulator transition in vanadium dioxide VO_2: A critical review, Comptes Rendus Phys. 22 (2021) 37–87. doi:10.5802/crphys.74.

[9] H. Lu, S. Clark, Y. Guo, J. Robertson, The metal-insulator phase change in vanadium dioxide and its applications, J. Appl. Phys. 129 (2021) 240902. doi:10.1063/5.0027674.

[10] J.B. Goodenough, The two components of the crystallographic transition in VO_2, J. Solid State Chem. 3 (1971) 490–500. doi:10.1016/0022-4596(71)90091-0.

[11] P. Shvets, O. Dikaya, K. Maksimova, A. Goikhman, A review of Raman spectroscopy of vanadium oxides, J. Raman Spectrosc. 50 (2019) 1226–1244. doi:10.1002/jrs.5616.

[12] M.G. Krishna, Y. Debauge, A.K. Bhattacharya, X-ray photoelectron spectroscopy and spectral transmittance study of stoichiometry in sputtered vanadium oxide films, Thin Solid Films. 312 (1998) 116–122. doi:10.1016/s0040-6090(97)00717-7.

[13] E. Hryha, E. Rutqvist, L. Nyborg, Stoichiometric vanadium oxides studied by XPS, Surf. Interface Anal. 44 (2012) 1022–1025. doi:10.1002/sia.3844.

[14] Z. Cao, S. Li, W. Xie, G. Du, Z. Qiao, Critical evaluation and thermodynamic optimization of the V-O system, Calphad: Comput. Coupling Ph. Diagr. Thermochem. 51 (2015) 241–251. doi:10.1016/j.calphad.2015.10.003.

[15] Y.-B. Kang, Critical Evaluation and Thermodynamic Optimization of the VO–$VO_{2.5}$ System, J. Eur. Ceram. Soc. 32 (2012) 3187–3198. doi:10.1007/s11663-020-01939-0.

[16] J. Outón, E. Blanco, M. Domínguez, H. Bakkali, J.M. Gonzalez-Leal, J.J. Delgado, M. Ramírez-del-Solar, Tracking the optical constants of porous vanadium dioxide thin films during metal–insulator transition: Influence of processing conditions on their application in smart glasses, Appl. Surf. Sci. 580 (2022) 152228. doi:10.1016/j.apsusc.2021.152228.

[17] Y. Zhang, W. Xiong, W. Chen, Y. Zheng, Recent progress on vanadium dioxide nanostructures and devices: Fabrication, properties, applications and perspectives, Nanomaterials. 11 (2021) 338. doi:10.3390/nano11020338.

[18] W. Wu, C. Wang, C. Chen, J. Song, F. Ma, Design of antireflection and enhanced thermochromic properties of TiO_2/VO_2 thin films, Adv. Mater. Interfaces. 10 (2023) 2202506. doi:10.1002/admi.202202506.

[19] K. Liu, S. Lee, S. Yang, O. Delaire, J. Wu, Recent progresses on physics and applications of vanadium dioxide, Mater. Today. 21 (2018) 875–896. doi:10.1016/j.mattod.2018.03.029.

[20] A.M. Alcaide, G. Regodon, F.J. Ferrer, V. Rico, R. Alvarez, T.C. Rojas, A.R. González-Elipe, A. Palmero, Low temperature nucleation of thermochromic VO_2 crystal domains in nanocolumnar porous thin films, Nanotechnology. 34 (2023) 255702. doi:10.1088/1361-6528/acc664.

[21] J. Liang, X. Yu, Y. Zhao, X. Fan, W. Wu, S. Wang, Enhancement of metal-insulator transition performance of VO_2 thin films by conventional furnace annealing, Thin Solid Films. 730 (2021) 138709. doi:10.1016/j.tsf.2021.138709.

[22] L. Pósa, G. Molnár, B. Kalas, Z. Baji, Z. Czigány, P. Petrik, J. Volk, A rational fabrication method for low switching-temperature VO_2, Nanomaterials. 11 (2021) 212. doi:10.3390/nano11010212.

[23] A. Annadi, M. Bohra, V. Singh, Modulations in electrical properties of sputter deposited vanadium oxide thin films: Implication for electronic device applications, Thin Solid Films. 758 (2022) 139451. doi:10.1016/j.tsf.2022.139451.

[24] P. Ashok, Y.S. Chauhan, A. Verma, Effect of vanadium thickness and deposition temperature on VO_2 synthesis using atmospheric pressure thermal oxidation, Thin Solid Films. 724 (2021) 138630. doi:10.1016/j.tsf.2021.138630.

[25] A.J. Santos, N. Martin, J. Outón, E. Blanco, R. García, F.M. Morales, A simple two-step approach to the fabrication of VO_2-based coatings with unique thermochromic features for energy-efficient smart glazing, Energy Build. 285 (2023) 112892. doi:10.1016/j.enbuild.2023.112892.

[26] A.J. Santos, N. Martin, J. Outón, E. Blanco, R. García, F.M. Morales, Towards the optimization of a simple route for the fabrication of energy-efficient VO_2-based smart coatings, Sol. Energy Mater. Sol. Cells. 254 (2023) 112253. doi:10.1016/j.solmat.2023.112253.

[27] M.M. Hawkeye, M.J. Brett, Glancing angle deposition: Fabrication, properties, and applications of micro- and nanostructured thin films, J. Vac. Sci. Technol. A. 25 (2007) 1317–1335. doi:10.1116/1.2764082.

[28] A. Barranco, A. Borras, A.R. Gonzalez-Elipe, A. Palmero, Perspectives on oblique angle deposition of thin films: From fundamentals to devices, Prog. Mater. Sci. 76 (2016) 59–153. doi:10.1016/j.pmatsci.2015.06.003.

[29] S. Dou, J. Zhao, W. Zhang, H. Zhao, F. Ren, L. Zhang, X. Chen, Y. Zhan, Y. Li, A universal approach to achieve high luminous transmittance and solar modulating ability simultaneously for vanadium dioxide smart coatings via

double-sided localized surface plasmon resonances, ACS Appl. Mater. Interfaces. 12 (2020) 7302–7309. doi:10.1021/acsami.9b17923.

[30] M. Kong, K. Egbo, C.P. Liu, M.K. Hossain, C.Y. Tso, C.Y. Hang Chao, K.M. Yu, Rapid thermal annealing assisted facile solution method for tungsten-doped vanadium dioxide thin films on glass substrate, J. Alloys Compd. 833 (2020) 155053. doi:10.1016/j.jallcom.2020.155053.

[31] J. Liang, S. Wang, D. Lei, Z. Wang, X. Li, Enhanced visible and tunable infrared transmittance of W-doped VO_2/SiO_2/PVP composite films for smart windows, Opt. Mater. 121 (2021) 111485. doi:10.1016/j.optmat.2021.111485.

[32] N. Shen, S. Chen, R. Shi, S. Niu, A. Amini, C. Cheng, Phase transition hysteresis of tungsten doped VO_2 synergistically boosts the function of smart windows in ambient conditions, ACS Appl. Electron. Mater. 3 (2021) 3648–3656. doi:10.1021/acsaelm.1c00550.

[33] T. Palomar, E. Enríquez, Evaluation of the interaction of solar radiation with colored glasses and its thermal behavior, J. Non. Cryst. Solids. 579 (2022) 121376. doi:10.1016/j.jnoncrysol.2021.121376.

[34] A.J. Santos, B. Lacroix, M. Domínguez, R. García, N. Martin, F.M. Morales, Controlled grain-size thermochromic VO_2 coatings by the fast oxidation of sputtered vanadium or vanadium oxide films deposited at glancing angles, Surfaces and Interfaces. 27 (2021) 101581. doi:10.1016/j.surfin.2021.101581.

[35] A.J. Santos, B. Lacroix, F. Maudet, A. Corvisier, F. Paumier, C. Dupeyrat, T. Girardeau, R. García, F.M. Morales, Surface oxidation of amorphous Si and Ge slanted columnar and mesoporous thin films: Evidence, scrutiny and limitations for infrared optics, Appl. Surf. Sci. 493 (2019) 807–817.

doi:10.1016/j.apsusc.2019.07.064.

[36] F.M. Morales, M. Escanciano, M.P. Yeste, A.J. Santos, Reactivity of vanadium nanoparticles with oxygen and tungsten, Nanomaterials. 12 (2022) 1471. doi: 10.3390/nano12091471.

[37] A.J. Santos, M. Escanciano, A. Suárez-Llorens, M.P.Yeste, F.M. Morales, A novel route for the easy production of thermochromic VO_2 nanoparticles, Chem. - A Eur. J. 27 (2021) 16662–16669. doi:10.1002/chem.202102566.

[38] M.M. Margoni, S. Mathuri, K. Ramamurthi, R.R. Babu, K. Sethuraman, Sprayed vanadium pentoxide thin films: Influence of substrate temperature and role of HNO_3 on the structural, optical, morphological and electrical properties, Appl. Surf. Sci. 418 (2017) 280–290. doi:10.1016/j.apsusc.2017.02.039.

[39] A. Baltakesmez, C. Aykaç, B. Güzeldir, Phase transition and changing properties of nanostructured V_2O_5 thin films deposited by spray pyrolysis technique, as a function of tungsten dopant, Appl. Phys. A Mater. Sci. Process. 125 (2019) 441. doi:10.1007/s00339-019-2736-0.

[40] A.J. Santos, N. Martin, J.J. Jiménez, R. Alcántara, S. Margueron, A. Casas-Acuña, R. García, F.M. Morales, Facile fabrication of high-performance thermochromic VO_2-based films on Si for application in phase-change devices, Chem. Mater. 35 (2023) 4435–4448. doi:10.1021/acs.chemmater.3c00613.

[41] D.S. Su, M. Wieske, E. Beckmann, A. Blume, G. Mestl, R. Schlögl, Electron beam induced reduction of V_2O_5 studied by analytical electron microscopy, Catal. Letters. 75 (2001) 81–86. doi:10.1023/A:1016754922933.

[42] A. Gloter, V. Serin, C. Turquat, C. Cesari, C. Leroux, G. Nihoul, Vanadium

valency and hybridization in V-doped hafnia investigated by electron energy loss spectroscopy, Eur. Phys. J. B. 22 (2001) 179–186. doi:10.1007/PL00011142.

[43] C. Hébert, M. Willinger, D.S. Su, P. Pongratz, P. Schattschneider, R. Schlögl, Oxygen K-edge in vanadium oxides: Simulations and experiments, Eur. Phys. J. B. 28 (2002) 407–414. doi:10.1140/epjb/e2002-00244-4.

[44] X. Zhou, Y. Meng, T.D. Vu, D. Gu, Y. Jiang, Q. Mu, Y. Li, B. Yao, Z. Dong, Q. Liu, Y. Long, A new strategy of nanocompositing vanadium dioxide with excellent durability, J. Mater. Chem. A. 9 (2021) 15618–15628. doi:10.1039/d1ta02525b.

[45] T.D. Vu, H. Xie, S. Wang, J. Hu, X. Zeng, Y. Long, Durable vanadium dioxide with 33-year service life for smart windows applications, Mater. Today Energy. 26 (2022) 100978. doi:10.1016/j.mtener.2022.100978.

[46] J.H. Yu, S.H. Nam, J.W. Lee, D.I. Kim, J.H. Boo, Selective near infrared transmittance control of thermochromic VO_2 thin films through colloidal lithography, Appl. Surf. Sci. 477 (2019) 22–26. doi:10.1016/j.apsusc.2018.02.243.

[47] L. Kang, Y. Gao, Z. Zhang, J. Du, C. Cao, Z. Chen, H. Luo, Effects of annealing parameters on optical properties of thermochromic VO_2 films prepared in aqueous solution, J. Phys. Chem. C. 114 (2010) 1901–1911. doi:10.1021/jp909009w.

[48] S. Chen, H. Zhang, High visible transmittance of VO_2 film prepared by DC magnetron sputtering with situ annealing, J. Opt. 50 (2021) 508–511. doi:10.1007/s12596-021-00719-6.

[49] D. Zomaya, W.Z. Xu, B. Grohe, S. Mittler, P.A. Charpentier, Bimodal size distribution of VO_2 nanoparticles in hydrophilic polymer films for temperature-triggered infrared transmission control, ACS Appl. Nano Mater. 3 (2020) 6645–6653. doi:10.1021/acsanm.0c01072.

[50] Y. Gao, H. Luo, Z. Zhang, L. Kang, Z. Chen, J. Du, M. Kanehira, C. Cao, Nanoceramic VO_2 thermochromic smart glass: A review on progress in solution processing, Nano Energy. 1 (2012) 221–246. doi:10.1016/j.nanoen.2011.12.002.

[51] J.Y. Suh, R. Lopez, L.C. Feldman, R.F. Haglund, Semiconductor to metal phase transition in the nucleation and growth of VO_2 nanoparticles and thin films, J. Appl. Phys. 96 (2004) 1209–1213. doi:10.1063/1.1762995.

[52] A. Gupta, R. Aggarwal, P. Gupta, T. Dutta, R.J. Narayan, J. Narayan, Semiconductor to metal transition characteristics of VO_2 thin films grown epitaxially on Si (001), Appl. Phys. Lett. 95 (2009) 111915. doi:10.1063/1.3232241.

[53] L. Chen, X. Wang, D. Wan, Y. Cui, B. Liu, S. Shi, H. Luo, Y. Gao, Tuning the phase transition temperature, electrical and optical properties of VO_2 by oxygen nonstoichiometry: Insights from first-principles calculations, RSC Adv. 6 (2016) 73070–73082. doi:10.1039/c6ra09449j.

[54] H. Zhang, Z. Wu, Q. He, Y. Jiang, Preparation and investigation of sputtered vanadium dioxide films with large phase-transition hysteresis loops, Appl. Surf. Sci. 277 (2013) 218–222. doi:10.1016/j.apsusc.2013.04.028.

[55] G. Xu, P. Jin, M. Tazawa, K. Yoshimura, Thickness dependence of optical properties of VO_2 thin films epitaxially grown on sapphire (0001), Appl. Surf. Sci. 244 (2005) 449–452. doi:10.1016/j.apsusc.2004.09.157.

[56] J. Bian, M. Wang, H. Sun, H. Liu, X. Li, Y. Luo, Y. Zhang, Thickness-modulated metal–insulator transition of VO_2 film grown on sapphire substrate by MBE, J. Mater. Sci. 51 (2016) 6149–6155. doi:10.1007/s10853-016-9863-1.

[57] A.J. Santos, N. Martin, J. Outón, A. Casas-Acuña, E. Blanco, R. García, F.M. Morales, Atmospheric flash annealing of low-dimensional vanadium nanolayers sputtered on glass substrates, Surfaces and Interfaces. 34 (2022) 102313. doi:10.1016/j.surfin.2022.102313.

[58] J. Qi, D. Zhang, Q. He, L. Zeng, Y. Liu, Z. Wang, A. Zhong, X. Cai, F. Ye, P. Fan, Independent regulation of electrical properties of VO_2 for low threshold voltage electro-optic switch applications, Sensors Actuators A Phys. 335 (2022) 113394. doi:10.1016/j.sna.2022.113394.